

## A 2D semi-analytical analysis of the time-dependent settlement of a shallow foundation placed near the soil slope

Hadi Haghgouei<sup>1</sup>, Ali Reza Kargar<sup>\*2</sup>, Mohammad Hossein Khosravi<sup>2</sup>, Mehdi Amini<sup>3</sup>

1- School of Mining Engineering, College of Engineering, University of Tehran, Iran

2- Assistant professor, School of Mining Engineering, College of Engineering, University of Tehran, Iran

3- Rock Mechanics Specialist, Thurber Engineering Ltd., Vancouver, British Columbia, Canada

\* Corresponding Author: *ar.kargar@ut.ac.ir*

(Received: August 2021 , Accepted: December 2021)

### Keywords

**Shallow foundation settlement**  
**Creep**  
**Time-dependent behavior**  
**Soil bearing capacity**  
**2D semi-analytical method**  
**Finite difference method**  
**Differential Settlement**

### Abstract

To assess the safety of the foundation, the ultimate bearing capacity, as well as the settlement of the footing, should be studied. The bearing capacity of a footing built near the slope has been widely investigated. However, the published research work which focused on the settlement of the footing close to the slope is very limited. In many cases, the foundations should be built adjacent to a slope. Since geomaterial behavior is usually time-dependent, and due to the limited published research work on the time-dependent settlement of the foundation on a slope, in this study, a semi-analytical method has been used to obtain the elastic and viscoelastic

settlement of a foundation rested on a slope. The proposed method has been developed based on the theory of elasticity by combining a transformed Airy stress function and finite difference method. To facilitate the use of the proposed solution, as well as investigating the effect of slope characteristics and footing geometry on the settlement, a set of elastic and time-dependent settlement charts have been proposed. The results indicate that the slope angle, the normalized footing distance from the crest, and the slope height play a prominent role in the settlement behavior of footing. By increasing the normalized footing distance or decreasing the slope angle, the settlement of the edges of the foundation tends to be equal and the behavior like a footing rested on a horizontal ground surface can be observed. Also, by decreasing the height of the slope, this behavior, i.e. behave like a footing on half-space, will happen in the smaller normalized footing distance.

### 1- INTRODUCTION

When the safety of a foundation is a matter of concern, two critical aspects should be considered: ultimate bearing capacity and the settlement of the foundation [1]. Indeed, the magnitude of foundation settlements, rotation as well as differential settlement should be restricted [2]. The elastic and time-dependent settlement of the foundation resting on a half-space has been investigated by many researchers [3-9]. In the case of settlement of the flexible foundation placed on an elastic horizontal ground surface, a solution that can give vertical settlement of inner and outer sides of the ring plate was developed by Fisher (1957) [3]. Egorov and Nichiporovich (1961) by employing Bessel's function, proposed an expression to compute the settlement and the stress under inflexible ring footings [4]. An analytical solution has been proposed by Gazetas et al. (1985) for evaluating the vertical elastic settlement of the footing [5]. Choobbasti et al. (2010) considered elasto-plastic analysis in FEM to simulate the settlement of ring foundation [6]. Naseri and Hosseininia (2015) studied the elastic settlement of ring

foundations by employing the FDM method [7]. Gunerathne et al. (2018) proposed a semi-analytical elastic method to evaluate the settlement of elastic tanks resting on a half-space soil medium [8]. In the case of elastic settlement, artificial neural networks have been employed by Diaz et al. (2018) to study the three-dimensional elastic settlement of the footing resting on soil and inclined bedrock [9]. Also, the long-term settlement of the footing has been studied by researchers. Taylor and Merchant (1940) by considering the soil mass as a Kelvin body examined the creep settlement of a footing [10]. Biot (1956) proposed an equation to study the viscoelastic deformation of a porous medium that is containing a viscous fluid [11]. Booker and Small (1986) investigated the long-term settlement of footing resting on a horizontal soil layer by transforming the governing equation [12]. Xie et al. (2008) examined the creep settlement of the footing subjected to time depending loading by considering the burger model [13]. To investigate the time-dependent behavior of clay, an elastic-viscoplastic equation was proposed by Yin et al. (2010) [14]. Zou et al. (2018) proposed a semi-analytical method to study the consolidation of clay by

considering the clay as an elastic-viscoplastic material [15]. Chen and Ai (2020) studied the viscoelastic behavior of transversely isotropic multilayered porous rock foundation by using numerical methods [2]. As is evident from the above-mentioned literature, the settlement of the footing resting on a horizontal ground surface has been widely studied. Regardless of many published research work that focuses on the investigating of the bearing capacity of a footing near the slope [16-22], to the knowledge of authors, the settlement of the footing placed close to the slope has been rarely investigated. Footing sometimes should be built on or near the slope [16, 17, 21, 23-26], and estimation of the foundation settlement is necessary for the design of shallow foundations [27]. Therefore, the study of footing settlement placed adjacent to the slope, to increase the safety of the structures, is amply clear. When the settlement assessment of shallow foundations is a matter of concern, it is common practice to consider both elastic and long-term settlement [7]. On the other hand, geomaterials deformation is a time-dependent phenomenon and demonstrate rheological behavior [2, 28-34], and therefore, to increase the safety of the structure, besides the elastic settlement, the study of time-dependent behavior of footing is of great importance in geotechnical engineering. In the literature, viscoelastic, elastic-viscoplastic, or elastoplastic-viscoplastic models have been used by researchers to investigate the time-dependent settlement of the foundation [35-38]. When the stress state in geomaterial is low, viscoelastic models can examine the time-dependent behavior more satisfactorily [39]. In the case of higher loading, where the geomaterials exhibit plastic deformation, the assessment of the bearing capacity of the foundation adjacent to a slope is more prominent than the evaluation of the settlement of the foundation, especially in the absence of supporting systems such as the retaining wall. In this research, a new approach that can consider all the effective parameters that play a significant role in the viscoelastic settlement of the foundation will be proposed to obtain both elastic and creep settlement of a footing adjacent to a slope. In this

regard, the slope and footing geometry, as well as the elastic and viscosity parameters of the slope material, will be taken into account. Also, to describe the time-dependent behavior of the soil or rock mass, the Burgers four-element model has been considered. It should be noted that, although numerical modeling can solve complex problems under various situations, due to time-consuming procedures it is not a cost-effective option in the initial stage of the design. In this study, the slope's material was considered as a homogeneous viscoelastic material. Also, the footing was considered as a shallow foundation with no embedment, and the interface between the foundation and the slope was assumed to be rough.

## 2- Detail of the proposed approach

### 2-1- Analytical part- Computing the stress and strain

Consider the footing resting on a slope, as presented in figure 1. The authors, proposed a new analytical method to evaluate the stress state due to loads of foundation, within a slope with high accuracy by considering a transformed Airy stress function [22]. The proposed transformed Airy stress function, as well as the stress components, are presented in Equations (1) and (2), respectively. To elaborate details on Equations (1) and (2) and the way of calculating them, interested readers are referred to the author's recently published research work [22, 40]

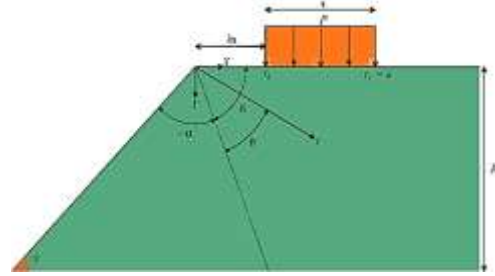


Fig. 1-. Schematic representation of the foundation resting near the slope

$$\Phi(z, \theta) = \frac{F(z)}{2z(z+1)} \left[ \frac{z \sin(z\alpha) \cos(z+2)\theta - (z+2) \sin(z+2)\alpha \cos(z\theta)}{(z+1) \sin(2\alpha) + \sin 2(z+1)\alpha} + \frac{(z+2) \cos(z+2)\alpha \sin(z\theta) - z \cos(z\alpha) \sin(z+2)\theta}{(z+1) \sin(2\alpha) - \sin 2(z+1)\alpha} \right] \quad (1)$$

$$\begin{aligned} (\sigma_\theta - \sigma_r) &= \frac{\lambda x}{r\pi} \left[ \int_0^\infty (g_1 + g_2) \left[ \text{Sin} \left( y \text{Log} \left( \frac{\lambda x}{r} \right) \right) \right] dy \right] - \frac{a}{r\pi} \left[ \int_0^\infty (g_1 + g_2) \left[ \text{Sin} \left( y \text{Log} \left( \frac{a}{r} \right) \right) \right] dy \right] + \left[ \text{Residu} \right] \frac{a - \lambda x}{r\pi} \\ (\sigma_\theta + \sigma_r) &= \frac{\lambda x}{r\pi} \left[ \int_0^\infty \frac{(g_5 y + g_3) + (g_6 y + g_4)}{1 + y^2} \text{Cos} \left( y \text{Log} \left( \frac{\lambda x}{r} \right) \right) dy + \int_0^\infty \frac{(g_3 y - g_5) + (g_4 y - g_6)}{1 + y^2} \text{Sin} \left( y \text{Log} \left( \frac{\lambda x}{r} \right) \right) dy \right] \\ &\quad - \frac{a}{r\pi} \left[ \int_0^\infty \frac{(g_5 y + g_3) + (g_6 y + g_4)}{1 + y^2} \text{Cos} \left( y \text{Log} \left( \frac{a}{r} \right) \right) dy \right] \\ &\quad + \int_0^\infty \frac{(g_3 y - g_5) + (g_4 y - g_6)}{1 + y^2} \text{Sin} \left( y \text{Log} \left( \frac{a}{r} \right) \right) dy - \left[ \text{Residu} \right] \frac{a - \lambda x}{r\pi} \\ \tau_{r\theta} &= \frac{\lambda x}{2r\pi} \int_0^\infty (g_7 - g_8) \text{Cos} \left( y \text{Log} \left( \frac{\lambda x}{r} \right) \right) dy - \frac{a}{2r\pi} \int_0^\infty (g_7 - g_8) \text{Cos} \left( y \text{Log} \left( \frac{a}{r} \right) \right) dy \end{aligned} \quad (2)$$

The functions  $g_1$  to  $g_8$  are defined in Appendix A. The role of dead load due to gravity has been neglected in the proposed method. However, based on the superposition approach, the gravity stress distribution in a slope suggested by Goodman and Brown (1963) has been added to the outcome of the

$$\begin{aligned}\sigma_{xx} &= \frac{\rho g}{\alpha - \tan(\alpha)} [Y(\alpha - \sin(\alpha)\cos(\alpha)) - 2\sin(\alpha)\cos^2(\alpha)(X\sin(\alpha) - Y\cos(\alpha))\log\left(\frac{\sin(\alpha - \beta)}{\sin(\alpha)}\right) - \\ &\quad \beta\sin(\alpha)[Y\sin(\alpha)(1 + 2\cos^2(\alpha)) + X\cos(\alpha)(1 - 2\sin^2(\alpha))] \\ \sigma_{yy} &= \rho g y - \frac{\rho g}{\alpha - \tan(\alpha)} [-Y\sin(\alpha)\cos(\alpha) + 2\sin^3(\alpha)(X\sin(\alpha) - Y\cos(\alpha))\log\left(\frac{\sin(\alpha - \beta)}{\sin(\alpha)}\right) \\ &\quad + \beta\sin(\alpha)[Y\sin(\alpha)(1 - 2\cos^2(\alpha)) + X\cos(\alpha)(1 + 2\sin^2(\alpha))] \\ \sigma_{xy} &= \frac{-\rho g}{\alpha - \tan(\alpha)} [Y\sin^2(\alpha) + 2\cos(\alpha)\sin^2(\alpha)(X\sin(\alpha) - Y\cos(\alpha))\log\left(\frac{\sin(\alpha - \beta)}{\sin(\alpha)}\right) \\ &\quad + \beta\sin(\alpha)(1 - 2\sin^2(\alpha))(X\sin(\alpha) - Y\cos(\alpha))]\end{aligned}\quad (3)$$

$$\text{where } \beta = \tan^{-1} \frac{Y}{X}.$$

As it is clear there is no exact solution to solve the integrals in Equation (2), and therefore the Filon [42] integration scheme was employed to calculate the stress components. The Filon numerical integration approach is presented in Appendix B. Total vertical time-dependent strain due to footing load may be represented by Equation (4) as follows,

$$\begin{aligned}\epsilon &= \epsilon_{dev} + \epsilon_v \\ \epsilon_v &= \frac{I_1}{9K} \\ \epsilon_{dev} &= \frac{1}{2G^*(t)} \sigma_{dev}\end{aligned}\quad (4)$$

In Equation (4) the subscript  $V$  and  $dev$  represent the volumetric and deviatoric strain, respectively.  $I_1$  denotes the first invariant of the stress tensor,  $K$  is the Bulk modulus, and  $G^*(t)$  is the time-dependent modulus. This modulus can be represented for Maxwell, Kelvin, and Burger model by Equations (5), (6), and (7), respectively.

$$\frac{1}{G_M^*(t)} = \frac{1}{G_M} + \frac{t}{\eta_M} \quad (5)$$

$$\frac{1}{G_K^*(t)} = \frac{1}{G_K} \left(1 - e^{-\frac{G_K t}{\eta_K}}\right) \quad (6)$$

$$\frac{1}{G_B^*(t)} = \frac{1}{G_M^*(t)} + \frac{1}{G_K^*(t)} \quad (7)$$

where  $\eta$  and  $G$  are the viscosity and shear modulus respectively. It should be noted that in this study, plane strain condition was considered, and therefore, the first invariant of stress may be computed as  $I_1 = (1 + \nu)(\sigma_x + \sigma_y)$ . Since this paper aims to examine the creep settlement of the foundation, it will be assumed that the stress state remains constant during the time.

## 2-2- Numerical part-Computing the settlement

To calculate the settlement of the footing rested on the slope, the Finite Difference Method was used. The slope domain has been meshed such that at each

newly proposed method, and therefore, the role of gravity is also considered in this study [41]. Equation (3) may represent the Goodman and Brown gravity stress  $g_8$  equation.

grid point, the vertical displacement was calculated through Equation (8).

$$\epsilon = \frac{\partial V}{\partial y} = \frac{V(y+h) - V(y)}{h} \quad (8)$$

where  $h$  and  $v$  are the size of the mesh and the vertical displacement, respectively.

## 3- Validation of the accuracy of the proposed method

To verify the semi-analytical solution, the results of the proposed method were compared with the outcome of COMSOL finite element commercial software. In this regard, two slope configurations have been modeled and two different material properties were assigned to the models. The slope characteristic and material properties are presented in Tables 1 and 2, respectively. Also, the poisson ratio of 0.3 was implemented into the model.

**Table 1-. The configuration of the modeled slope**

Case	Slope angle	$H/x$	$\lambda$
1	45	10	0
2	30	5	1

**Table 2-. Visco-elastic parameters of studied cases**

Case	$G_M$ (Pa)	$G_K$ (Pa)	$\eta_M$ (Pa.s)	$\eta_K$ (Pa.s)	Ref.
1	7.6e6	1.8e5	1.08e16	1.08e15	[43, 44]
2	1.2e7	7.5e8	1.0e15	9.7e21	[44, 45]

The settlement of the two edges and center of the footing was monitored during the time. The comparison between the proposed method and COMSOL FEM software is presented in Figure 2. A good agreement is evident between the outcome of numerical simulation and the suggested method.

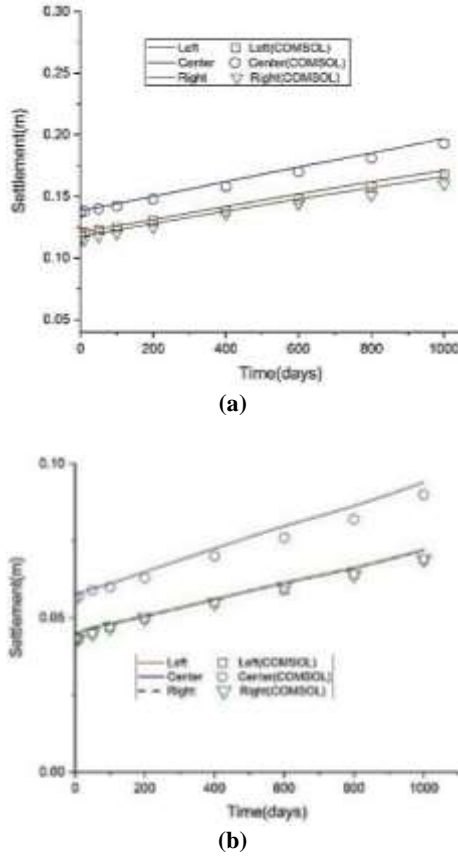


Fig. 2-. The edges and center settlement of the footing are placed at (a) 45-degree slope with  $H/x=10$  and  $\lambda=0$  and (b) 30-degree slope with  $H/x=5$  and  $\lambda=1$ .

#### 4- Analysis of the creep settlement of the foundation near the slope based on slope characteristics

To study the creep settlement of the foundation built near the slope in more detail an attempt will be made to propose a set of charts. Equation (4) will be divided into three parts, elastic, Maxwell, and Kelvin strain. This will help to take the slope geometry, material properties, and foundation loading into proposed charts. In this section, the details of the separation of Equation (4) and the definition of differential settlement of the foundation will be introduced. Then, the introduced methodology will be used in the next section in the form of some charts and the results will be discussed in detail.

##### 4-1- Elastic vertical strain

The first part refers to elastic strain which is illustrated in Equation (9) as follows,

$$\begin{aligned} \epsilon^e &= \frac{1}{2G} \left( \sigma_y - \frac{I_1}{3} \right) + \frac{I_1}{9k} \\ &= \frac{-\nu(1+\nu)}{E} \sigma_x \\ &\quad + \frac{1-\nu^2}{E} \sigma_y \end{aligned} \quad (9)$$

Equation (9) can be subdivided into Equations (10) and (11) to normalize the strain based on the material properties (i.e.  $\nu$  and  $E$ ).

$$\epsilon^e_1 = \frac{-\nu(1+\nu)}{E} \sigma_x \quad (10)$$

$$\epsilon^e_2 = \frac{1-\nu^2}{E} \sigma_y \quad (11)$$

##### 4-2- Maxwell viscous strain

Maxwell strain can be represented by Equation (12) where the last part denotes the elastic strain.

$$\begin{aligned} \epsilon^M &= \frac{1}{2G_M} \frac{t}{\tau_M} \left( \sigma_y - \frac{I_1}{3} \right) \\ &\quad + \left( \frac{1}{2G_M} \left( \sigma_y - \frac{I_1}{3} \right) + \frac{I_1}{9K} \right) \end{aligned} \quad (12)$$

Where  $\tau_M = \frac{\eta_M}{G_M}$ . The elastic strain was calculated in the elastic vertical strain subsection, and therefore, the elastic part of the Maxwell strain will be neglected here.

To normalize the Maxwell viscous strain based on the material properties, the Maxwell Equation can be divided into the two parts as follows,

$$\begin{aligned} \epsilon^M &= \epsilon^M_1(t, G_M, \tau_M, \sigma_y) \\ &\quad + \epsilon^M_2(t, G_M, \tau_M, \nu, \sigma_y, \sigma_x) \end{aligned} \quad (13)$$

Where

$$\epsilon^M_1 = \frac{1}{2G_M} \frac{t}{\tau_M} \sigma_y$$

$$\epsilon^M_2 = \frac{-(1+\nu)}{6G_M} \frac{t}{\tau_M} (\sigma_x + \sigma_y)$$

##### 4-3- Kelvin strain

Kelvin strain is represented in Equation (14). Following the same strategy as the previous section, the kelvin strain is also divided into two parts as follows,

$$\begin{aligned} \epsilon^K &= \epsilon^K_1(t, G_K, \tau_K, \sigma_y) + \epsilon^K_2(t, G_K, \tau_K, \nu, \sigma_y, \sigma_x) \\ &= \frac{1}{2G_K} \left( 1 - e^{-\frac{t}{\tau_K}} \right) \left( \sigma_y - \frac{I_1}{3} \right) \end{aligned} \quad (14)$$

Where

$$\epsilon^K_1 = \frac{1}{2G_K} \left( 1 - e^{-\frac{t}{\tau_K}} \right) \sigma_y$$

$$\epsilon^K_2 = \frac{-(1+\nu)}{6G_K} \left( 1 - e^{-\frac{t}{\tau_K}} \right) (\sigma_x + \sigma_y)$$

##### 4-4- Settlement evaluation

The settlement of a foundation can be categorized into three modes: uniform settlement, planar tilt, and differential settlement. The angular distortion, as a type of differential settlement, can consider the effect of footing width [8], and therefore was used in this paper. To evaluate the differential settlement (angular distortion) Equations (15) to (17) were used. It should be noted that the vertical

displacement of the center, left and right sides of the foundation (i.e.  $V_C$ ,  $V_L$ , and  $V_R$ ) is calculated based on Equation (8). Equations (15) and (16) evaluate the normalized differential settlement of the left and right sides of the footing respectively concerning the center of the footing. A normalized differential settlement between the left and right sides of the footing can be calculated through Equation (17).

$$\Delta_{CL} = \frac{V_C - V_L}{x/2} \quad (15)$$

$$\Delta_{CR} = \frac{V_C - V_R}{x/2} \quad (16)$$

$$\Delta_{LR} = \frac{V_L - V_R}{x} \quad (17)$$

In Equations (15) to (17) Subscript L, R and C denote the Left, right, and center of the footing respectively as shown in Figure 1.

### 5- Details of the analysis

The elastic and time-dependent normalized differential settlement (angular distortion) of the footing adjacent to the slope has been calculated based on section 4 and will be presented here as some charts. In this research, the slope angles of 10, 20, 30, 45, 60, 70, 80, and 90 were considered. Also, to investigate the effect of slope height on the settlement of the foundations, two normalized slope heights,  $H/x=10$  and 4 were studied. Moreover, the normalized distance from the crest of the slope was considered from  $\lambda=0$  to 2. Based on the selected model, i.e. elastic, Kelvin, Maxwell, or Burgers, researchers can use these charts as following instructions:

For the assessment of elastic settlement, the charts in the elastic settlement should be used. In the case where the Maxwell model was chosen, the sum of elastic settlement and viscose part of the Maxwell model should be considered. Also, when the Kelvin model was selected, the charts in the Kelvin settlement section can be taken into account. Finally, if the Burgers model was chosen, the sum of all three sections should be considered. It should be noted that, for each body (i.e. elastic, Maxwell, or Kelvin), the sum of  $\Delta_1$  and  $\Delta_2$  (i.e. the sum of two vertical axes) must be considered. Both vertical axes are normalized based on the elastic and viscous properties of the masses, and the foundation loading. Therefore, the charts will represent the effect of slope and footing geometry on the settlement. Another advantage of normalizing is that charts can be used based on the desired material properties and loading. In this regard,  $\Delta^*_i$  was defined (presented in Table 3) and will be used to normalize the differential settlement (angular distortion) of the foundation.

A flowchart describing the solution steps of the problem is illustrated in Fig. 3.

Table 3-. Definition of  $\Delta^*_i$  based on material properties and foundation loading

$(\Delta^*_e)_1$	$(\Delta^*_e)_2$	$(\Delta^*_M)_1$	$(\Delta^*_M)_2$	$(\Delta^*_K)_1$	$(\Delta^*_K)_2$
$\frac{\nu(1+\nu)}{0.3125 l}$	$\frac{(1-\nu^2)_i}{0.9375 l}$	$\frac{P}{2.5 G_M}$	$\frac{P}{3.125 G_l}$	$\frac{P}{G_K}$	$\frac{P}{1.25 G_K}$

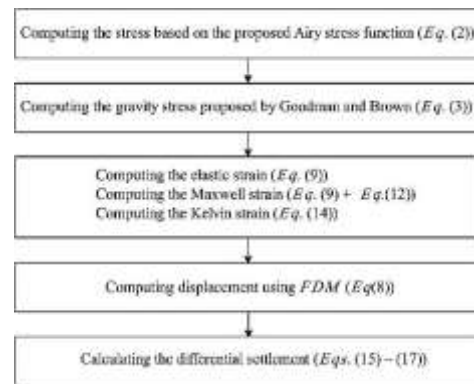


Fig. 3-. solution steps of the problem

### 5-1- Elastic Settlement

Fig. 4 represents the normalized elastic differential settlement of the foundation adjacent to the slope with  $H/x=10$ . From this figure, it can be concluded that by increasing the slope angle and decreasing the normalized distance from the crest of the slope,  $\Delta_{CL}$  is also decreased and for 80 and 90-degree slope angle,  $\Delta_{CL}$  will be negative when  $\lambda$  is smaller than 0.5. This indicates that the settlement of the left side is greater than the center of the footing and maximum settlement occurs on the left side of the foundation. Also, the settlement on the left side is greater than the right side, and therefore, as illustrated in Fig. 4-c foundation tends to topple to the left side (the occurrence of the toppling failure depends on the height of the structure to the width of the foundation). Also, by increasing the  $\lambda$  value, the settlement curve for all slope angle tend to approach the same value. This indicates the fact that by increasing the  $\lambda$  value, the effect of slope angle will vanish and the same behavior of foundation on the half-space will occur. As can be seen from Figure 4-c the curves represent the differential settlement between the left and right sides of the footing is approaching zero for all slope angles. By decreasing the slope angle and slope height this behavior (i.e. the behavior of a footing resting on the horizontal ground surface) will occur at a lower  $\lambda$ . Figures 5, 6, and 7 represent the elastic settlement of the foundation for  $H/x=7$ , 4, and 1 respectively. By considering the curves that demonstrate 80 and 90-degree slopes in Figure 4-c, it can be concluded beyond the  $\lambda$  greater than two, the differential settlement is not equal to zero. However, as can be seen in figure 5-c, the curve represents an 80-degree slope that is almost equal to zero at  $\lambda=2$ . By decreasing the normalized slope height to 4 (i.e.  $h/x=4$ ) in Figure 6-c, all curves tend to reach zero

value beyond the  $\lambda$  greater than 1.5. Also, when  $h/x=1$  (see Figure 7-c) all curves almost reach zero value at  $\lambda=1$ . Table 4 represents the differential settlement between the left and right sides of the footing for the 60-degree slope at  $\lambda=1.5$ . As can be seen by decreasing the slope normalized height, the value of differential settlement tends to reach zero.

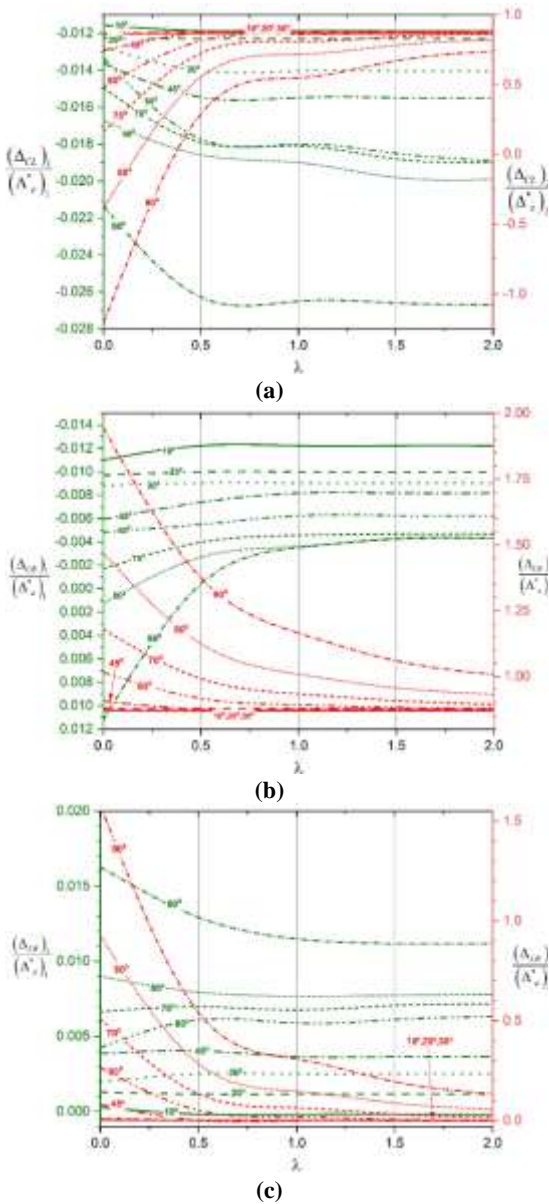


Fig. 4-. Variation of differential elastic settlement of a footing with normalized distance from the crest for  $H/x=10$  (a) left to center differential settlement (b) right to center differential settlement (c) left to right differential settlement

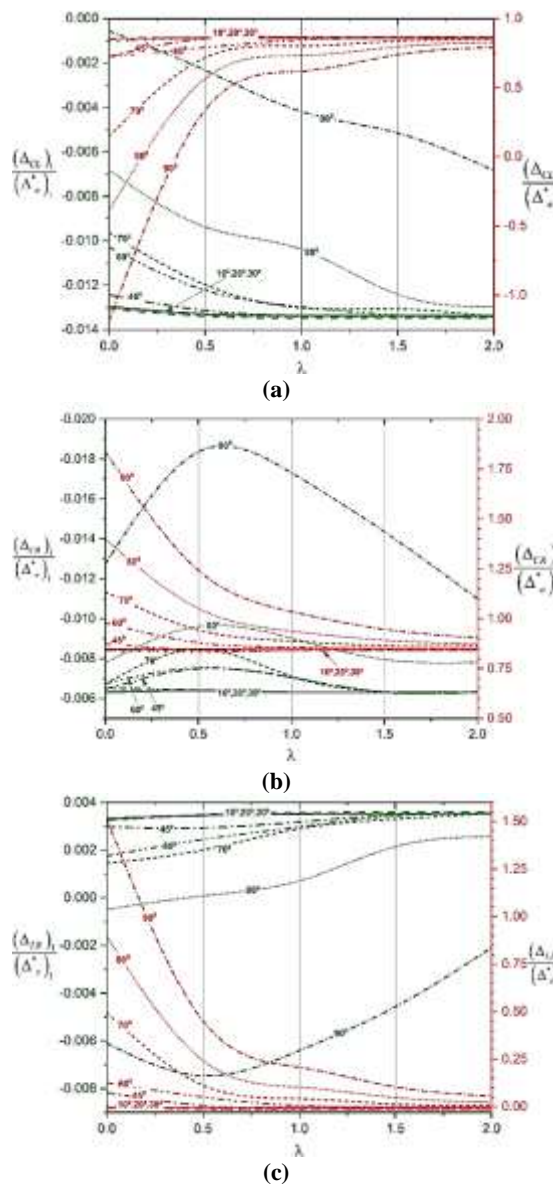


Fig. 5-. Variation of differential elastic settlement of a footing with normalized distance from the crest for  $H/x=7$  (a) left to center differential settlement (b) right to center differential settlement (c) left to right differential settlement

Table 4-. Decreasing the differential settlement between the left and right sides of the footing to zero by decreasing the slope height for a 60-degree slope and at  $\lambda=1.5$

Normalized height ( $H/x$ )	slope	$\frac{(\Delta_{LR})_1}{(\Delta_e^*)_1}$	$\frac{(\Delta_{LR})_2}{(\Delta_e^*)_2}$
10		6.12e-3	4.81e-3
7		3.55e-3	2.6e-3
4		6.95e-4	5.55e-4
1		5e-6	2.2e-4

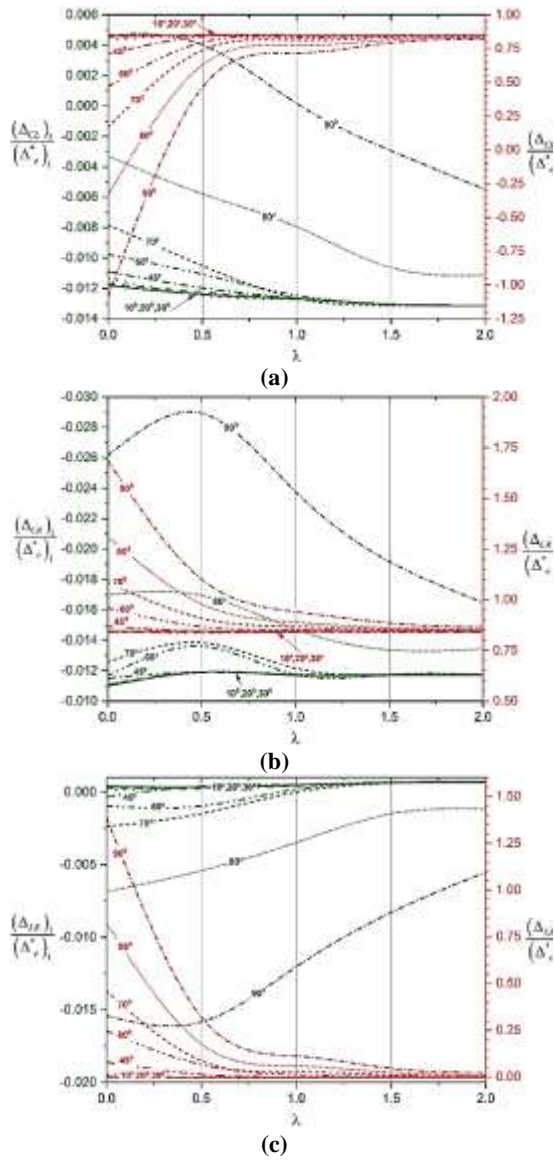


Fig. 6-. Variation of differential elastic settlement of a footing with normalized distance from the crest for  $H/x=4$  (a) left to center differential settlement (b) right to center differential settlement (c) left to right differential settlement

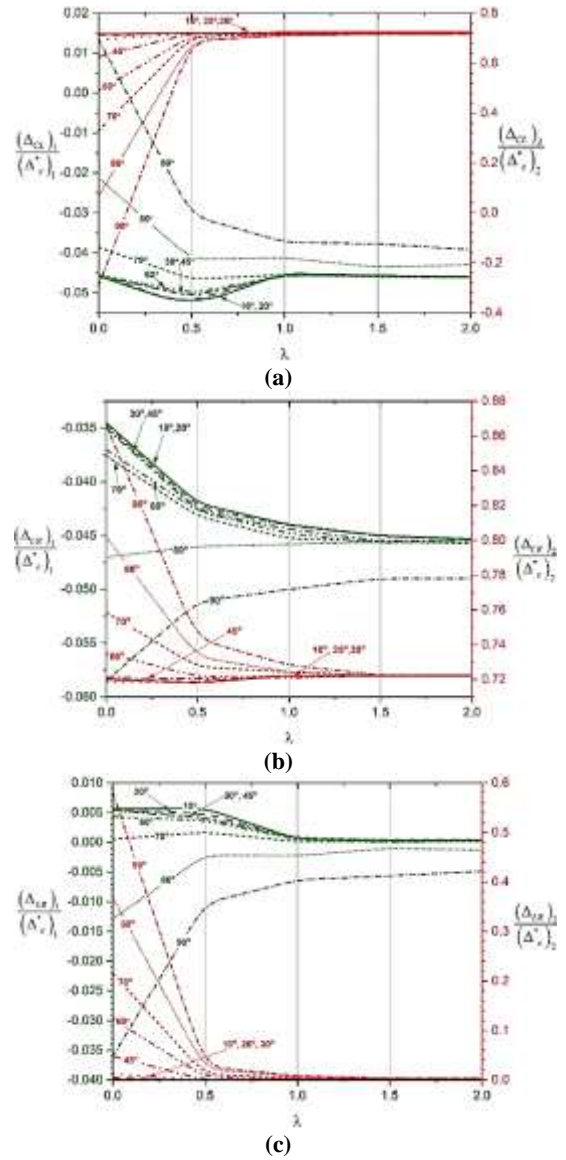
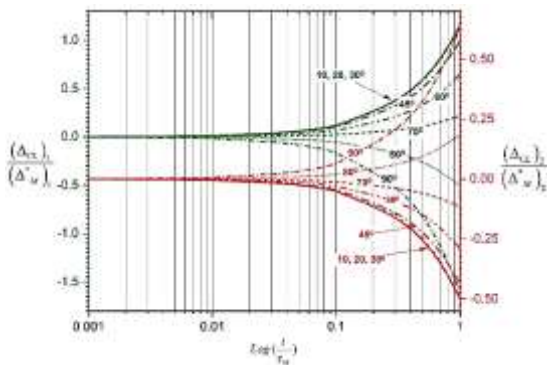


Fig. 7-. Variation of differential elastic settlement of a footing with normalized distance from the crest for  $H/x=1$  (a) left to center differential settlement (b) right to center differential settlement (c) left to right differential settlement

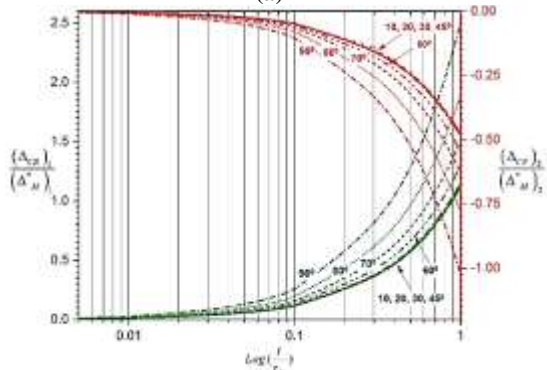
**5-2- Viscose part of Maxwell settlement**

In this section Maxwell model was considered to evaluate the creep settlement. It should be noted that, as discussed in section 3, the elastic part of the Maxwell model is obtained in section 5.1 and here just the viscose part will be discussed. Figs. 8 to 10 represent the  $\Delta_{CL}$ ,  $\Delta_{CR}$ , and  $\Delta_{LR}$  for the  $H/x=10$  and different  $\lambda$ . As can be seen in Fig. 8,  $\Delta_{CL}$  for 80 and 90 degrees slope is negative. This indicates that, for these angles, the settlement of the left edge of the foundation is greater than the center of footing. Figs.

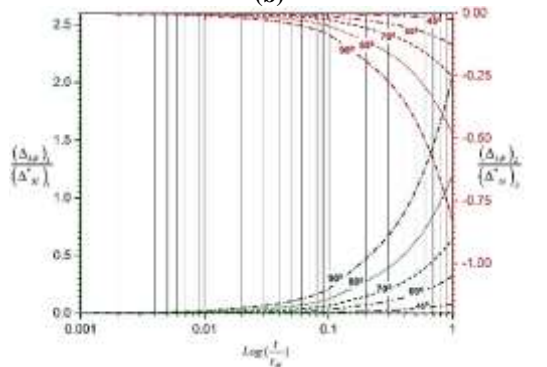
9 and 10 indicate that by increasing the distance of the footing from the crest,  $\Delta_{CL}$  becomes positive and the effect of slope angle on the settlement is also decreased. By increasing the  $\lambda$ , the effect of slope geometry will diminish and as discussed previously, the behavior like a footing on half-space can be observed. Fig. 10-c manifested that, for slope angles of 10, 20, 30, 45, 60, and 70 degrees, the settlement on both sides of the foundation is equal. Also, by decreasing the slope height, as presented in Figures C-1 to C-3 in Appendix C, this behavior will occur at a lower  $\lambda$ .



(a)

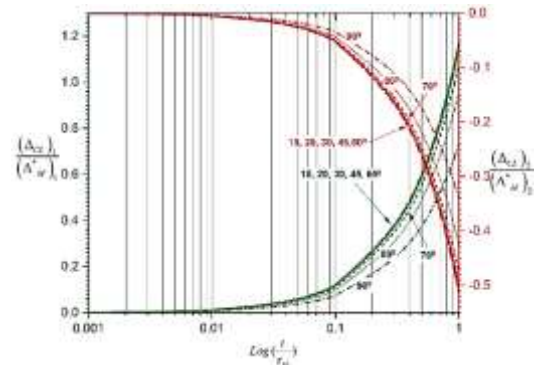


(b)

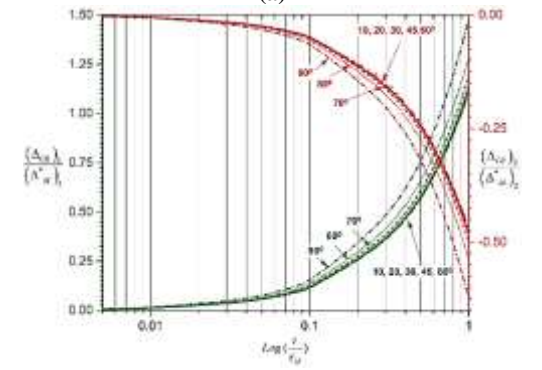


(c)

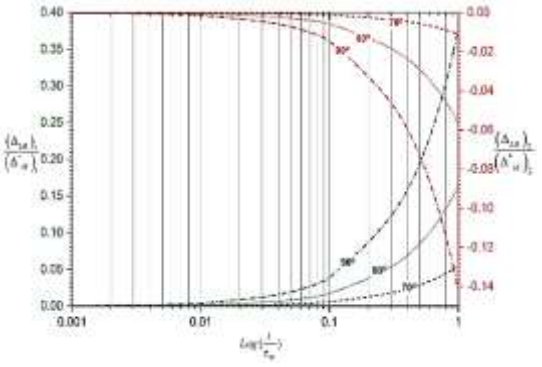
Fig. 8-. Variation of differential viscous part of Maxwell model settlement of a footing with time for  $\lambda=0$   $H/x=10$  (a) left to center differential settlement (b) right to center differential settlement (c) left to right differential settlement



(a)

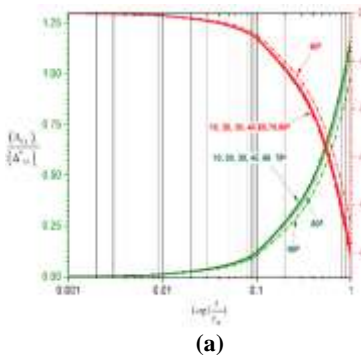


(b)

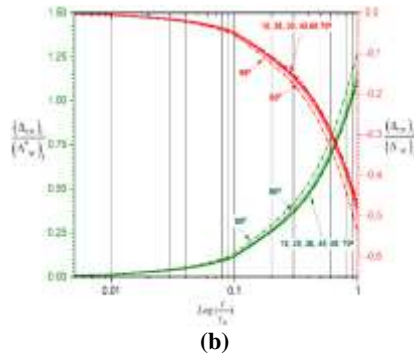


(c)

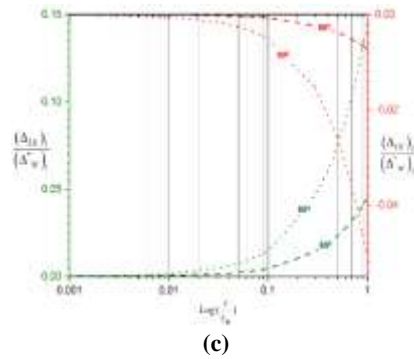
Fig. 9-. Variation of differential viscous part of Maxwell model settlement of a footing with time for  $\lambda=1$   $H/x=10$  (a) left to center differential settlement (b) right to center differential settlement (c) left to right differential settlement



(a)



(b)



(c)

Fig. 10-. Variation of differential viscous part of Maxwell model settlement of a footing with time for  $\lambda=2$   $H/x=10$  (a) left to center differential settlement (b) right to center differential settlement (c) left to right differential settlement

### 5-3- Kelvin settlement

The same trend of the Maxwell viscous part can be observed here. Fig. 11 illustrated that for 80 and 90 degrees the  $\Delta_{CL}$  is negative and the foundation tends to forward topple. Also, by increasing the  $\lambda$  value, or decreasing the slope height, the effect of slope geometry will diminish. Fig. 12 shows the variation of differential Kelvin model settlement of a footing with time for  $\lambda=1$  and  $H/x=10$ . Fig. 13-c demonstrates that, for slope angles of 10, 20, 30, 45, 60, and 70 degrees, the settlement on both sides of the foundation are approximately equal.

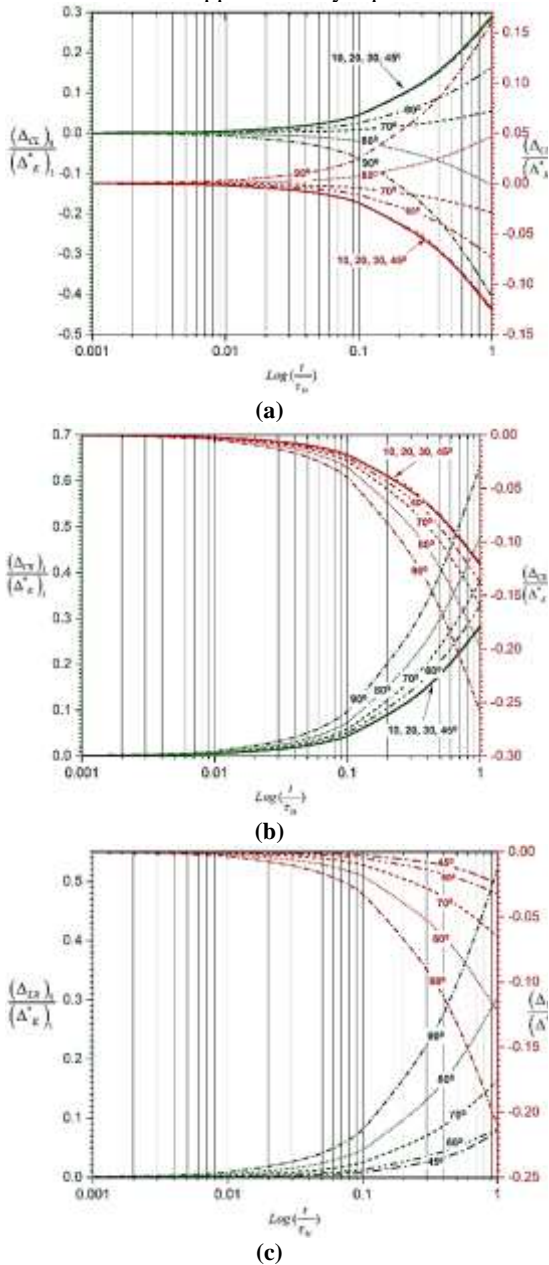


Fig. 11- Variation of differential Kelvin model settlement of a footing with time for  $\lambda=0$ ,  $H/x=10$  (a) left to center differential settlement (b) right to center differential settlement (c) left to right differential settlement

The charts for the normalized slope height of 4 are presented in Figs. C-4 to C-6 in Appendix C. As can be seen in these figures, regardless of the slope angle all the curves tend to converge into one for the settlement of normalized slope height of 4 when  $\lambda=2$ .

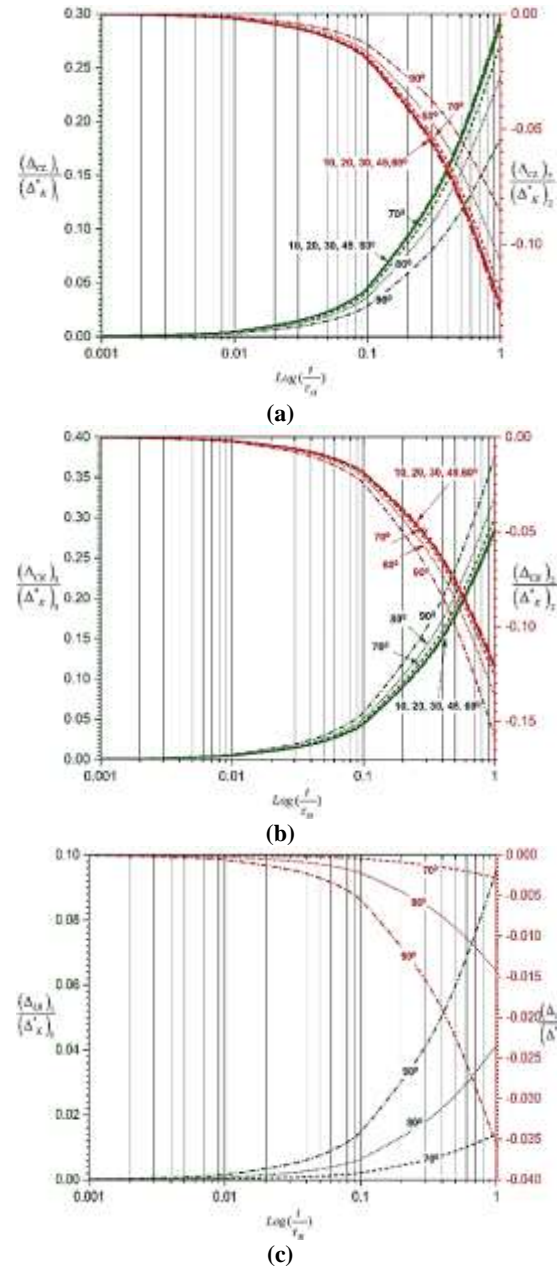


Fig. 12- Variation of differential Kelvin model settlement of a footing with time for  $\lambda=1$   $H/x=10$  (a) left to center differential settlement (b) right to center differential settlement (c) left to right differential settlement

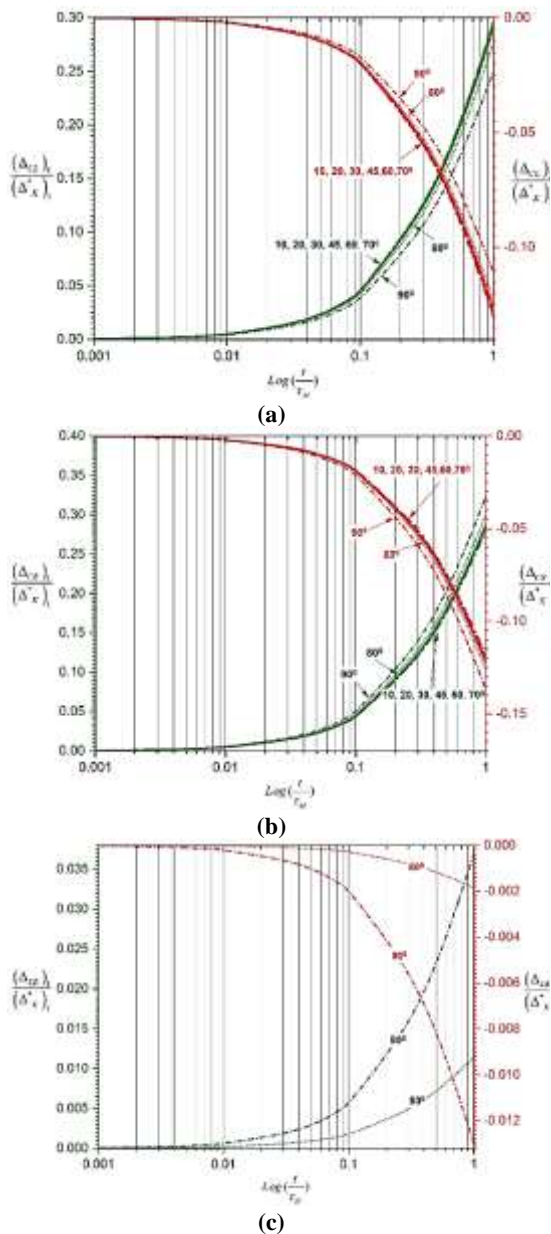


Fig. 13-. Variation of differential Kelvin model settlement of a footing with time for  $\lambda=2$   $H/x=10$  (a) left to center differential settlement (b) right to center differential settlement (c) left to right differential settlement.

**6- Conclusion**

One of the important aspects in the design stage of shallow foundation that should be taken into account is the differential settlement of the footing. Geomaterial demonstrates rheological behavior and its deformation is time-dependent [2, 28-34]. Because of the prominent role of footing settlement on the safety of the structures and the limited published study on the assessment of settlement, an attempt has been made to examine the time-dependent settlement of the footing adjacent to the slope. In this study, a 2D semi-analytical solution has been suggested. First, by using a developed Airy stress function, the stress component in the slope due

to foundation load has been obtained. Then by considering Hook’s law and four-element Burgers model the elastic and visco-elastic strain has been calculated. By combining the analytical method with the finite difference method, the differential settlement of the foundation based on the different bodies (i.e. elastic, Maxwell, and Kelvin) has been assessed. To evaluate the accuracy of the proposed method in evaluating the settlement of the foundation, the results of the proposed method have been compared with COMSOL FEM commercial software. The comparison between the result of COMSOL FEM and the proposed method demonstrates a good agreement. To facilitate the use of the proposed method, some charts that can incorporate the elastic and viscose properties of the slope’s material, along with the slope and footing geometry, into the engineering design are proposed. The results indicate that the slope angle, the normalized footing distance from the crest, and the slope height play a prominent role in the settlement behavior of footing. By increasing the normalized footing distance or decreasing the slope angle, the settlement of the edges of the foundation tends to be equal, and beyond the  $\lambda$  greater than 2, the effect of slope geometry will diminish such that the behavior of footing rest on the horizontal ground surface will occur. Also, by decreasing the height of the slope, this behavior, i.e. behave like a footing on half-space, will happen in the smaller normalized footing distance. To sum up, for a foundation with  $\lambda$  greater than two and resting on a slope with an angle smaller than 80-degree, the slope geometry does not play a significant role in the settlement of the foundation.

**REFERENCE**

[1] Meyerhof G. The ultimate bearing capacity of foundations. *Geotechnique*. 1951;2(4):301-32.  
 [2] Chen YF, Ai ZY. Viscoelastic analysis of transversely isotropic multilayered porous rock foundation by fractional Poyting-Thomson model. *Eng Geol*. 2020;264(105327).  
 [3] Fisher K. Zur Berechnung der setzung Von Fundamenten in der form einer Kreisformigen Ringflache. *Der Bauingenieur*. 1957;32(5):172-4.  
 [4] Egorov K, Nichiporovich A. Research on the deflection of foundations. *Proceedings of the 5th international conference on soil mechanics and foundation engineering*1961. p. 861-6.  
 [5] Gazetas G, Tassoulas J, Dobry R, O’Rourke M. Elastic settlement of arbitrarily shaped foundations embedded in half-space. *Geotechnique*. 1985;35(3):339-46.  
 [6] Choobbasti A, Hesami S, Najafi A, Pirzadeh S, Farrokhzad F, Zahmatkesh A. Numerical evaluation of bearing capacity and settlement of ring footing; case study of Kazeroon cooling towers. *International Journal of Research and Reviews in Applied Sciences*. 2010;4(2).

- [7] Naseri M, Hosseininia ES. Elastic settlement of ring foundations. *Soils and Foundations*. 2015;55(2):284-95.
- [8] Gunerathne S, Seo H, Lawson WD, Jayawickrama PW. Analysis of edge-to-center settlement ratio for circular storage tank foundation on elastic soil. *Computers and Geotechnics*. 2018;102(136-47).
- [9] Díaz E, Brotons V, Tomás R. Use of artificial neural networks to predict 3-D elastic settlement of foundations on soils with inclined bedrock. *Soils and Foundations*. 2018;58(6):1414-22.
- [10] Taylor DW, Merchant W. A theory of clay consolidation accounting for secondary compression. *Journal of Mathematics and Physics*. 1940;19(1-4):167-85.
- [11] Biot MA. Theory of deformation of a porous viscoelastic anisotropic solid. *Journal of Applied physics*. 1956;27(5):459-67.
- [12] Booker JR, Small J. Finite layer analysis of viscoelastic layered materials. *International Journal for Numerical and Analytical Methods in Geomechanics*. 1986;10(4):415-30.
- [13] Xie KH, Xie XY, Li XB. Analytical theory for one-dimensional consolidation of clayey soils exhibiting rheological characteristics under time-dependent loading. *International journal for numerical and analytical methods in geomechanics*. 2008;32(14):1833-55.
- [14] Yin Z-Y, Chang CS, Karstunen M, Hicher P-Y. An anisotropic elastic-viscoplastic model for soft clays. *International Journal of Solids and Structures*. 2010;47(5):665-77.
- [15] Zou S-F, Li J-Z, Xie X-Y. A semi-analytical solution for one-dimensional elasto-viscoplastic consolidation of layered soft clay. *Applied Clay Science*. 2018;153(9-15).
- [16] Meyerhof G. The ultimate bearing capacity of foundations on slopes. *Proc, 4th Int Conf on Soil Mechanics and Foundation Engineering 1957*. p. 384-6.
- [17] Kusakabe O, Kimura T, Yamaguchi H. Bearing capacity of slopes under strip loads on the top surfaces. *Soils and foundations*. 1981;21(4):29-40.
- [18] Narita K, Yamaguchi H. Bearing capacity analysis of foundations on slopes by use of log-spiral sliding surfaces. *Soils and Foundations*. 1990;30(3):144-52.
- [19] Georgiadis K. Undrained bearing capacity of strip footings on slopes. *Journal of geotechnical and geoenvironmental engineering*. 2010;136(5):677-85.
- [20] Leshchinsky B. Bearing capacity of footings placed adjacent to  $c'-\phi'$  slopes. *Journal of geotechnical and geoenvironmental engineering*. 2015;141(6):04015022.
- [21] Zhou H, Zheng G, Yin X, Jia R, Yang X. The bearing capacity and failure mechanism of a vertically loaded strip footing placed on the top of slopes. *Computers and Geotechnics*. 2018;94(12-21).
- [22] Haghgoei H, Kargar AR, Amini M, Khosravi MH. Semianalytical Solution for Evaluating Bearing Capacity of a Footing Adjacent to a Slope. *International Journal of Geomechanics*. 2020;21(2):06020041.
- [23] Ni P, Wang S, Zhang S, Mei L. Response of heterogeneous slopes to increased surcharge load. *Computers and Geotechnics*. 2016;78(99-109).
- [24] Saran S, Sud V, Handa S. Bearing capacity of footings adjacent to slopes. *Journal of geotechnical engineering*. 1989;115(4):553-73.
- [25] Graham J, Andrews M, Shields D. Stress characteristics for shallow footings in cohesionless slopes. *Canadian Geotechnical Journal*. 1988;25(2):238-49.
- [26] Shields D, Chandler N, Garnier J. Bearing capacity of foundations in slopes. *Journal of geotechnical engineering*. 1990;116(3):528-37.
- [27] Bungenstab FC, Bicalho KV. Settlement predictions of footings on sands using probabilistic analysis. *Journal of Rock Mechanics and Geotechnical Engineering*. 2016;8(2):198-203.
- [28] Deng Q, Zhu Z, Cui Z, Wang X. Mass rock creep and landsliding on the Huangtupo slope in the reservoir area of the Three Gorges Project, Yangtze River, China. *Eng Geol*. 2000;58(1):67-83.
- [29] Cong L, Hu X. Triaxial rheological property of sandstone under low confining pressure. *Eng Geol*. 2017;231(45-55).
- [30] Malan D. Time-dependent behaviour of deep level tabular excavations in hard rock. *Rock Mech Rock Eng*. 1999;32(2):123-55.
- [31] Zeng Z, Kou X. Application of viscoelasticity to study the time-dependent surface subsidence caused by underground mining. *Eng Geol*. 1992;32(4):279-84.
- [32] Omar MN, Abbiss CP, Taha MR, Nayan KAM. Prediction of long-term settlement on soft clay using shear wave velocity and damping characteristics. *Eng Geol*. 2011;123(4):259-70.
- [33] Zhou X, Cheng H. The long-term stability analysis of 3D creeping slopes using the displacement-based rigorous limit equilibrium method. *Eng Geol*. 2015;195(292-300).
- [34] Yao Y-P, Qi S-J, Che L-W, Chen J, Han L-M, Ma X-Y. Postconstruction settlement prediction of high embankment of silty clay at Chengde airport based on one-dimensional creep analytical method: case study. *International Journal of Geomechanics*. 2018;18(7):05018004.
- [35] Christie I. A re-appraisal of Merchant's contribution to the theory of consolidation. *Geotechnique*. 1964;14(4):309-20.
- [36] Kaliakin VN, Dafalias YF. Theoretical aspects of the elastoplastic-viscoplastic bounding surface model for cohesive soils. *Soils and foundations*. 1990;30(3):11-24.
- [37] Yin J-H, Graham J. Equivalent times and one-dimensional elastic viscoplastic modelling of time-dependent stress-strain behaviour of clays. *Canadian Geotechnical Journal*. 1994;31(1):42-52.
- [38] Justo J, Durand P. Settlement-time behaviour of granular embankments. *International journal for numerical and analytical methods in geomechanics*. 2000;24(3):281-303.

[39] Zhu H-H, Liu L-C, Pei H-F, Shi B. Settlement analysis of viscoelastic foundation under vertical line load using a fractional Kelvin-Voigt model. *Geomechanics and Engineering*. 2012;4(1):67-78.

[40] Haghgoei H, Kargar AR, Amini M, Esmaili K. An analytical solution for analysis of toppling-slumping failure in rock slopes. *Eng Geol*. 2020;265(105396).

[41] Goodman L, Brown C. Dead load stresses and the instability of slopes. *Journal of the Soil Mechanics and Foundations Division*. 1963;89(3):103-36.

[42] Filon LNG. III.—On a Quadrature Formula for Trigonometric Integrals. *Proceedings of the Royal Society of Edinburgh*. 1930;49(38-47).

[43] Pellet FL. Large Time-Dependent Convergences In A Tunnel Excavated In A Carboniferous Rock Mass. *ISRM International Symposium-6th Asian Rock Mechanics Symposium: International Society for Rock Mechanics and Rock Engineering*, 2010.

[44] Paraskevopoulou C, Perras M, Diederichs M, Loew S, Lam T, Jensen M. Time-dependent behaviour of brittle rocks based on static load laboratory tests. *Geotechnical and Geological Engineering*. 2018;36(1):337-76.

[45] Paraskevopoulou C. Time-dependency of rocks and implications associated with tunnelling: *Queen's University (Canada)*, 2016.

**Appendix A-The functions  $g_1$  to  $g_8$  in Equation (2)**

$$g_1 = \frac{-\sin(\alpha-\theta) \cosh(\alpha+\theta)y + \sin(\alpha+\theta) \cosh(\alpha-\theta)y}{(y \sin 2\alpha - \sinh(2\alpha y))}$$

$$g_2 = \frac{\sin(\alpha+\theta) \cosh(\alpha-\theta)y + \sin(\alpha-\theta) \cosh(\alpha+\theta)y}{(y \sin 2\alpha + \sinh(2\alpha y))}$$

$$g_3 = \frac{-\cos(\alpha-\theta) \sinh(\alpha+\theta)y + \cos(\alpha+\theta) \sinh(\alpha-\theta)y}{(y \sin 2\alpha - \sinh(2\alpha y))}$$

$$g_4 = \frac{\cos(\alpha+\theta) \sinh(\alpha-\theta)y + \cos(\alpha-\theta) \sinh(\alpha+\theta)y}{(y \sin 2\alpha + \sinh(2\alpha y))}$$

$$g_5 = \frac{-\sin(\alpha-\theta) \cosh(\alpha+\theta)y + \sin(\alpha+\theta) \cosh(\alpha-\theta)y}{(y \sin 2\alpha - \sinh(2\alpha y))}$$

$$g_6 = \frac{\sin(\alpha+\theta) \cosh(\alpha-\theta)y + \sin(\alpha-\theta) \cosh(\alpha+\theta)y}{(y \sin 2\alpha + \sinh(2\alpha y))}$$

$$g_7 = \frac{\sin(\alpha-\theta) \sinh(\alpha+\theta)y + \sin(\alpha+\theta) \sinh(\alpha-\theta)y}{y \sin(2\alpha) - \sinh(2\alpha y)}$$

$$g_8 = \frac{\sin(\alpha-\theta) \sinh(\alpha+\theta)y - \sin(\alpha+\theta) \sinh(\alpha-\theta)y}{y \sin(2\alpha) + \sinh(2\alpha y)}$$

$$Residue = \left[ \frac{\pi \sin \alpha \cos \theta}{\sin 2\alpha - 2\alpha} + \frac{\pi \sin \alpha \cos \theta}{\sin 2\alpha + 2\alpha} \right]$$

**Appendix B-Filon numerical integration method**

$$\int_{x_0}^{x_{2n}} f(x) \cos(tx) dx = l[\Omega(tl)[f_{2n} \sin(tx_{2n}) - f_0 \sin(tx_0)] + \chi(tl)c_{2n} + \omega(tl)c_{2n-1}]$$

$$\int_{x_0}^{x_{2n}} f(x) \sin(tx) dx = l[\Omega(th)[-f_{2n} \cos(tx_{2n}) + f_{x_0} \cos(tx_0)] + \chi(tl)S_{2n} + \omega(tl)S_{2n-1}]$$

where,

$$c_{2n} = \left[ 2 \sum_{i=0}^n f_{2i} \cos(tx_{2i}) - [f_{2n} \cos(t x_{2n}) + f_0 \cos(tx_0)] \right]$$

$$c_{2n-1} = \sum_{i=1}^n f_{2i-1} \cos(tx_{2i-1})$$

$$S_{2n} = \left[ 2 \sum_{i=0}^n f_{2i} \sin(tx_{2i}) - [f_{2n} \sin(t x_{2n}) + f_0 \sin(tx_0)] \right]$$

$$S_{2n-1} = \sum_{i=1}^n f_{2i-1} \sin(tx_{2i-1})$$

$$\Omega(tl) = \frac{1}{tl} + \frac{\sin(2tl)}{2(tl)^2} - \frac{2\sin^2(tl)}{(tl)^3}$$

$$\chi(tl) = 2 \left[ \frac{1 + \cos^2(tl)}{(tl)^2} - \frac{\sin(2tl)}{(tl)^3} \right]$$

$$\omega(tl) = 4 \left[ \frac{\sin(tl)}{(tl)^3} - \frac{\cos(tl)}{(tl)^2} \right]$$

**Appendix C**

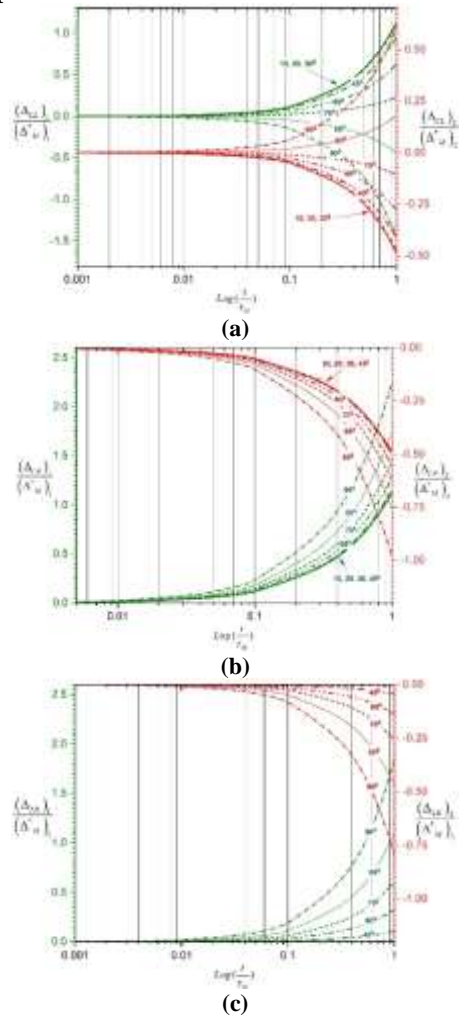


**Fig. 14-. C-1** Variation of differential viscose part of Maxwell model settlement of a footing with time for  $\lambda=0$ ,  $H/x=4$   
 (a) left to center differential settlement  
 (b) right to center differential settlement  
 (c) left to right differential settlement

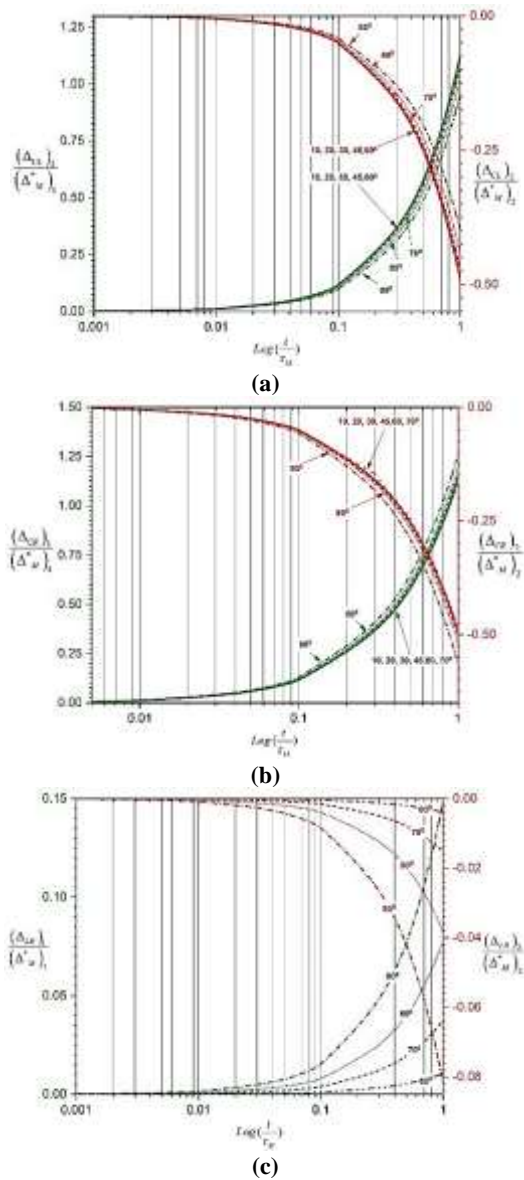


Fig. 15-. C-2 Variation of differential viscose part of Maxwell model settlement of a footing with time for  $\lambda=1$ ,  $H/x=4$   
 (a) left to center differential settlement  
 (b) right to center differential settlement  
 (c) left to right differential settlement

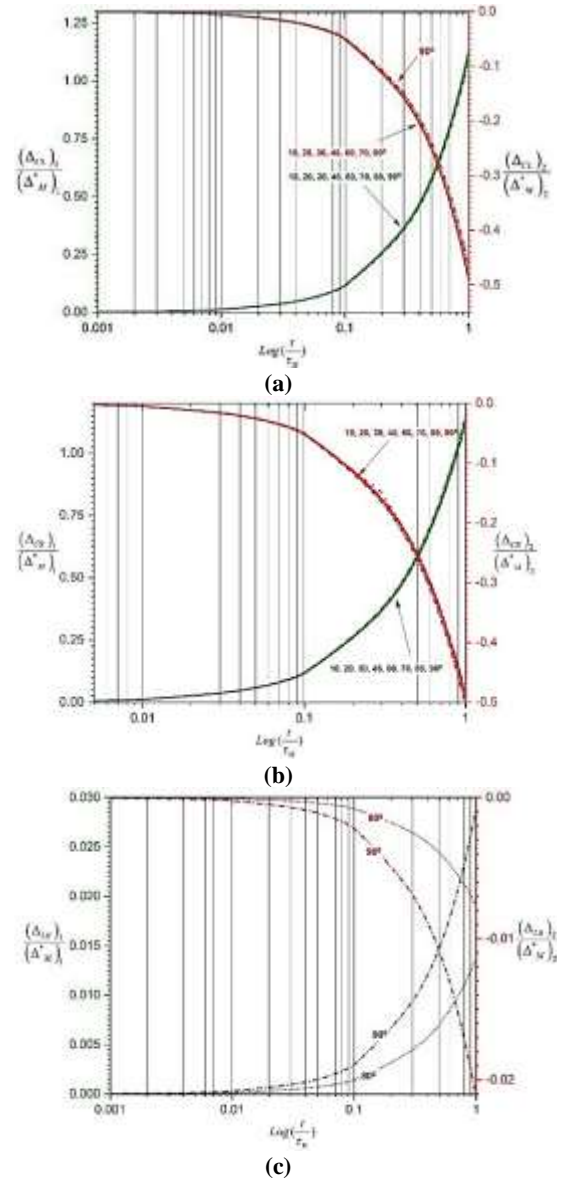


Fig. 16-. C-3 Variation of differential viscose part of Maxwell model settlement of a footing with time for  $\lambda=2$ ,  $H/x=4$   
 (a) left to center differential settlement  
 (b) right to center differential settlement  
 (c) left to right differential settlement

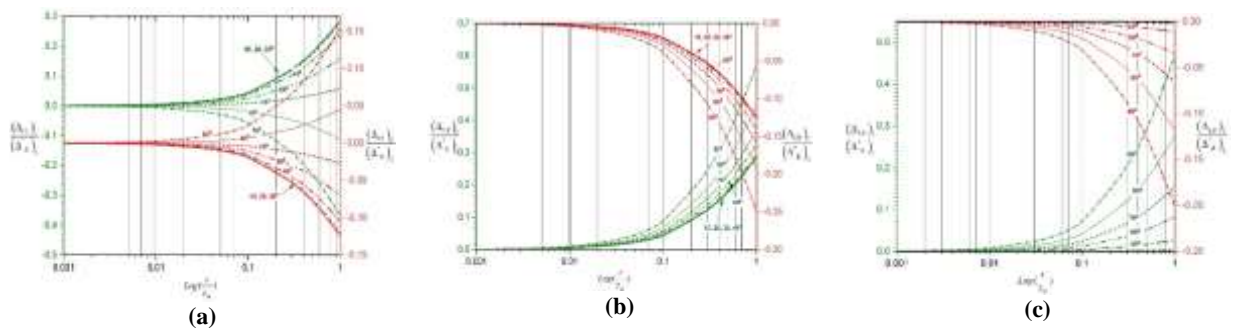
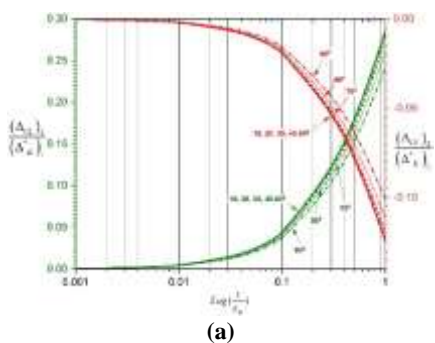
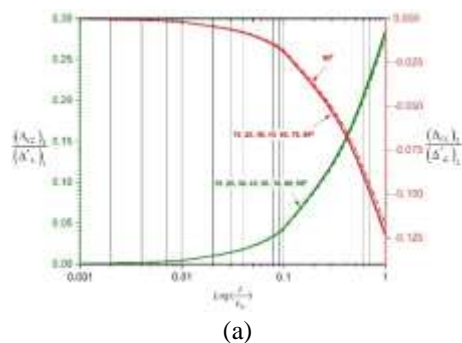


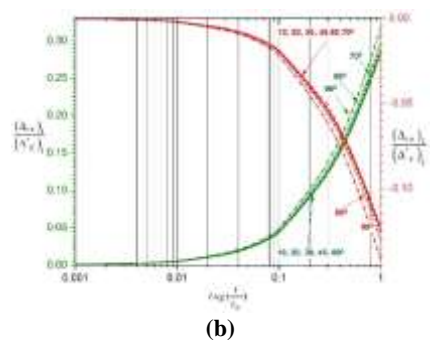
Fig. 17-. C-4 Variation of differential Kelvin model settlement of a footing with time for  $\lambda=0$   $H/x=4$  (a) left to center differential settlement (b) right to center differential settlement (c) left to right differential settlement



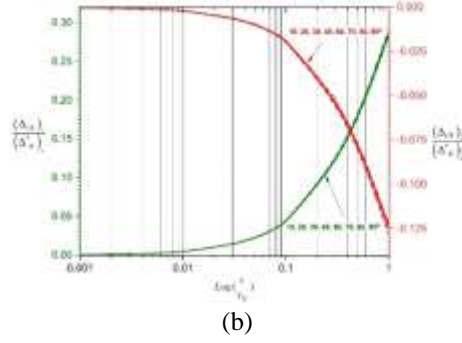
(a)



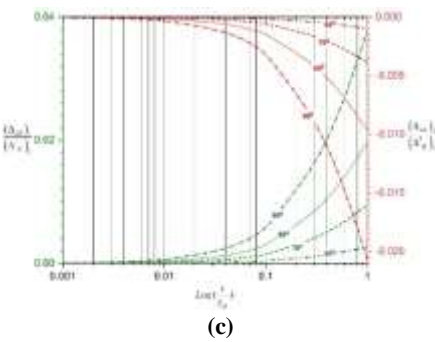
(a)



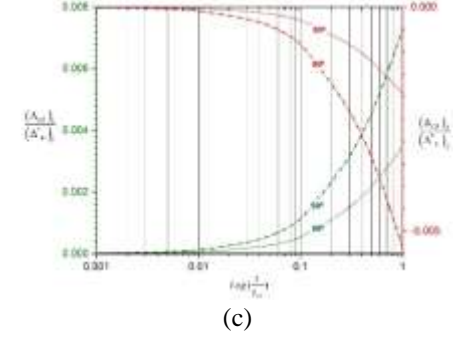
(b)



(b)



(c)



(c)

Fig. 18-. C-5 Variation of differential Kelvin model settlement of a footing with time for  $\lambda=1 H/x=4$   
 (a) left to center differential settlement  
 (b) right to center differential settlement  
 (c) left to right differential settlement

Fig. 19-. C-6 Variation of differential Kelvin model settlement of a footing with time for  $\lambda=2 H/x=4$   
 (a) left to center differential settlement  
 (b) right to center differential settlement  
 (c) left to right differential settlement